Applied Catalysis B: Environmental 303 (2022) 120901

Contents lists available at ScienceDirect

Applied Catalysis B: Environmental

journal homepage: www.elsevier.com/locate/apcatb

Increasing reactivity of plasmonic hot holes by a trapping strategy

Chaoyu Li [a,b], Zhiling Ma [a], Bing Han [a,b,c,*]

[a] College of Chemistry and Environmental Science, Hebei University, Baoding 071002, PR China
[b] Faculty of Veterinary and Agricultural Sciences, The University of Melbourne, Parkville, Victoria 3010, Australia
[c] Institute of Life Science and Green Development, Hebei University, Baoding 071002, PR China

ARTICLE INFO

Keywords:
Hydrogen
Hot carriers
Solar energy
Surface plasmons
Hot holes
Gold
Photocatalysis

ABSTRACT

Plasmonic photocatalysis has emerged as a promising solution for global energy crisis and environment pollution by facilitating wide ranging chemical transformations using photons in a broad region of solar spectrum. Despite numerous successful examples on improvement of electron-driven photochemistry, effective utilization of plasmonic hot holes is a long-standing challenge due to their ultrafast relaxation and short lifetime. Herein, we report that the reactivity of plasmonic hot holes can be greatly enhanced by a novel hot hole trapping strategy. We demonstrate a new concept of a metal-adsorbate interfacial structure that can be *in situ* constructed on gold (Au) surface in the presence of molecular hydrogen (H_2) under plasmonic excitation, where the key is to employ an electron-filled antibonding state hybridized by H1*s* and Au5*d* as a localized "trap" to improve utilization efficiency of plasmonic hot holes. This interfacial structure is evidenced by light-induced H_2 spillover and *d*-band model analysis. The prolonged lifetime and preserved oxidation power of plasmonic hot holes was evidenced by superior photocatalytic activity for methylene blue (MB) degradation in the presence of H_2 which was accelerated by over 5 times. In addition, FTIR coupled with CO molecular probe reveals that the physical location of hole trapping are low coordinated positions sites on Au nanoparticles. These findings could provide an innovative pathway to increase utilization efficiency of hot holes for visible-light-driven photocatalysis applications.

1. Introduction

Plasmonic nanoparticles (NPs) have appealed extensive attention in a wide scope of technological applications including medicine, sensing and photocatalysis owing to their unique optical properties [1,2]. Radiations with the highest photon flux of solar spectrum can be efficiently converted into high-energy electrons and holes by conducting electrons at the surface of gold nanoparticles (Au NPs) through surface plasmon resonance (SPR) phenomenon [3,4]. The hot electrons and holes are readily available to facilitate wide ranging chemical transformations, providing a promising solution for global energy crisis and environment pollution. Despite of excellent light-harvesting abilities, the photo-to-chemical conversion efficiencies of plasmonic materials are low, resulting from the ultrafast relaxation and recombination of hot charge carriers [2,5]. Therefore, research is increasingly focused on developing effective strategies to improve the reactivity of photogenerated carriers in plasmonic NPs [6].

Until now, the excited-state dynamics of charge carriers generated in plasmonic metals has been extensively studied. Effective electron extraction could be observed at the interfacial junctions when plasmonic metals were coupled with semiconductor, graphene or adsorbed molecules [7,8,43]. The lifetime of hot electrons in plasmonic metals can be prolonged via their injection across a Schottky barrier into the conduction band (CB) of *n*-type semiconductors [9]. However, a major challenge for plasmonic photocatalysts is the low utilization efficiency of hot holes due to their ultrashort lifetime, diffusion length and ultrafast relaxation [1,10,11]. According to theoretical calculation [10,12], the hot holes at <1.5 eV below the Fermi level (E_F) in plasmonic metals generated mainly by inter-band transition exhibit lifetime of only 10–40 fs and the mean free path length of 10–50 nm. Brongersma et al. [2] indicated that relaxation of hot holes into a Fermi-Dirac-like distribution only takes 100 fs to 1 ps due to electron-electron scattering. Although these relaxed holes with energy close to E_F (−5.20 V vs vacuum level) can oxidize sacrificial reagents [13], they are thermodynamically unfavorable for uphill reactions like water oxidation (−5.73 V vs vacuum level) [8]. Recently, limited successes have been made in organic transformation [14,15], metal oxidation [16], nano-deposition [17], and oxygen generation [18], by introducing metal-semiconductor or metal-molecule interfacial junction, to improve the oxidation potential of the plasmonic hot holes. Notably, those examples were still in low

* Corresponding author at: College of Chemistry and Environmental Science, Hebei University, Baoding 071002, PR China.
E-mail address: bing.han@unimelb.edu.au (B. Han).

https://doi.org/10.1016/j.apcatb.2021.120901
Received 5 September 2021; Received in revised form 17 October 2021; Accepted 3 November 2021
Available online 7 November 2021

efficacies or require assistance of external voltage [19]. The fundamental mismatch between the lifetime of hot holes (fs-ps) and the time scale of chemical transformations (ms-s), as well as the discrepancy between energy levels of hot holes and redox potentials of chemical reactions are long-standing challenges to realize the full potential of the plasmonic hot holes [1,20].

To overcome this issue, constructing effective nanostructures on plasmonic catalysts to prolong hot hole lifetime while preserving the oxidation potential is highly desirable. Nørskov et al. [21,22] employed density functional theory (DFT) calculations to describe the interaction between adsorbate valence states and the *s* and *d* states of a transition-metal surface, which indicated that the center of antibonding state of Au-H interaction is well below Fermi level (E_F) and largely filled by electrons. We thereby speculate that this antibonding state is available to act as a "trap" for photogenerated hot holes. Since the center of the antibonding state is considerably lower than E_F, the trapped hot holes are expected to possess higher oxidation energy than photogenerated hot holes relaxed to E_F. Moreover, the trapped hot holes can reduce the amounts of electrons at the antibonding state which in return stabilize Au-H interfacial structure.This hypothesis is consistent with the experimental observation that Au is chemically inert and inactive towards H_2 adsorption under dark conditions [23–25], but can form metastable gold hydride (AuH_x) under irradiation [26].

Herein, we report a novel trapping strategy for plasmonic hot holes based on adsorbate-metal interaction. Key to the success is the in-situ generation of localized electronic structure between Au NPs and adsorbed H_2 under visible light which is expected to enhance reactivity of plasmonic hot holes. As a proof-of-concept experimental study, visible-light photocatalytic degradation of methylene blue (MB) was employed as a model reaction to investigate the reactivity of plasmonic holes, where MB is one of the major contaminants in wastewater in a wide scope of industries [27]. Mechanism analysis was conducted using light-induced H_2 spillover by *in situ* FTIR, and *d*-band model analysis, and CO adsorption on Au NPs as a molecular probe.

2. Experimental

2.1. Sample preparation

Au/TiO_2 sample was fabricated via a well-established colloidal-photodeposition method as reported [28]. Briefly, to 750 mL aqueous tetrachloroauric acid ($HAuCl_4 \cdot 3H_2O$, Sigma-Aldrich, 520918-5g) solution (0.49 mmol L^{-1}), 100 cm^3 aqueous solution containing 39 mmol L^{-1} sodium citrate (Fisher Scientific BP327-500) was added. Then the solution was heated and boiled for 90 min under vigorous stirring, followed by cooling down to room temperature. TiO_2 Aeroxide™ P25 powder (Fisher Scientific Hampton, NH) was suspended in 20 mL of collected solution containing colloidal Au NPs (1.39 mg-Au/20 mL). Before the photoirradiation, a sacrificial reagent (20 mL) of methanol was added into the beaker. The mixture was photo-irradiated for 2 h by a 500 W high-pressure mercury arc (Newport, Irvine, CA) under magnetic stirring at room temperature. The resultant powder was washed repeatedly with centrifuge and NANOpure™ water for 5 times and then dried in an oven overnight. The next day the dried samples were crushed into powder in a porcelain boat and calcinated tube furnace at 300 °C for 2 h to remove possible organic contaminants.

2.2. Characterization

UV–vis diffuse reflectance spectra of Au/TiO_2 and TiO_2 were obtained on a UV-Vis spectrometer (Shimadzu UV-2600) at a range of 220–850 nm. $BaSO_4$ was chosen as a reflectance standard. Transmission electron microscopy (TEM) images were taken by JEOL 2010F. High Angle Annular Dark Field Scanning Transmission Electron Microscopy (HAADF-STEM) images were obtained with FEI Titan operated at 300 kV using SiN membranes and holey-C support films where measurements were taken from particles that were hanging over the holes and samples and membrane were plasma cleaned (ICP, Ar/O_2) for 9 s before taking image. Element mapping was obtained by Scanning Transmission Electron Microscopy coupled with electron energy loss spectroscopy (STEM-EELS).

2.3. Photocatalytic test

The photocatalytic activity of Au/TiO_2 samples was examined in a sealed cylindrical quartz container of 0.25 L volume (inner diameter of 5 cm and height of 12 cm), using a water recirculating system to keep temperature at 30 °C throughout the experiment. About 30 mg of the catalyst was dispersed in 70 mL of MB solution (10 mg/L). The catalyst adsorbs MB for 30 min while protected from light under stirring and gas bubbling to reach the adsorption-desorption equilibrium. Then the mixture was irradiated by a Xe lamp (PLS-SEX300, PerfectLight, Beijing) emitting white light coupled with 495 nm long pass filter coming from the top. The light intensity was measured to be around 400 mW cm^{-2}. Control experiments in dark were also performed under the same condition. This approach allows the selective excitation of the Au NPs while excluding any contribution from direct inter-band transitions within the TiO_2. The visible-light-driven activity of the photocatalysts was measured by monitoring the absorption intensity of MB at ~664 nm in a Shimadzu Shimadzu UV-2600 spectrophotometer as reported elsewhere [29–31]. After different reaction times, ~3.5 mL of solution sample was sourced from of the mixture and to measure the dye concentration. The photocatalytic reaction was fitted with Langmuir Hinshelwood model where its kinetics was expressed as $\ln(c_t/c_0) = -kt$ [29], where k is the apparent rate constant, and c_0 and c_t are the dye concentrations at initial state and after irradiation for t min, respectively. For detecting the active species in photodegradation process, hydroxyl radicals (·OH) and plasmon-induced hot holes (h^+) were examined by adding 1.0 mM IPA (a quencher of·OH) and TEOA (a quencher of h^+), respectively [29,30].

2.4. In situ FTIR analysis

IR spectra were obtained using a *in situ* diffuse reflectance infrared Fourier transform spectroscopy (DRIFTS, Thermo Scientific, Nicolet iS50) equipped with an MCT/A detector and ZeSe windows and a high temperature reaction chamber (Harrick Scientific Products, Inc). Before each experiment, about 10 mg of Au/TiO_2 catalyst was heated to 473 K in He flow (20 mL/min) for 30 min to get rid of adsorbed water molecule and then cooled down to at 30 °C for subsequent experiment. Before CO adsorption, the background spectrum was collected in flowing He (20 mL/min). Afterwards catalysts were first exposed to 1% CO/He (20 mL/min) for 30 min, followed by switching to pure H_2 (20 mL/min). During FTIR measurement, the sample was kept in dark or irradiated by a Xe lamp (PLS-SEX300, PerfectLight, Beijing) coupled with 495 nm long pass filter in H_2. The accuracy of temperature control is within 1 K which is achieved by a K-type thermocouple located under the tungsten sample grid. The purity of the H_2 and CO used was 99.999%. IR background and sample spectra were collected with 256 scans at 2 cm^{-1} resolutions, and the intensities were presented in Kubelka-Munk units.

3. Results and discussion

3.1. Characterization of Au/TiO_2 composite

Au/TiO_2 is a catalyst that has been extensively studied in both synthesis and photocatalysis and thus was used as a persuasive example here [32]. The morphology of pure Au NPs and Au/TiO_2 composite synthesized by colloidal photo-deposition method were examined by transmission electron microscopy (TEM) and High Angle Annular Dark Field Scanning Transmission Electron Microscopy (HAADF-STEM), respectively. One can see the as-prepared Au NPs demonstrate a morphology of nano-spheres in Fig. 1A. The statistical diameter

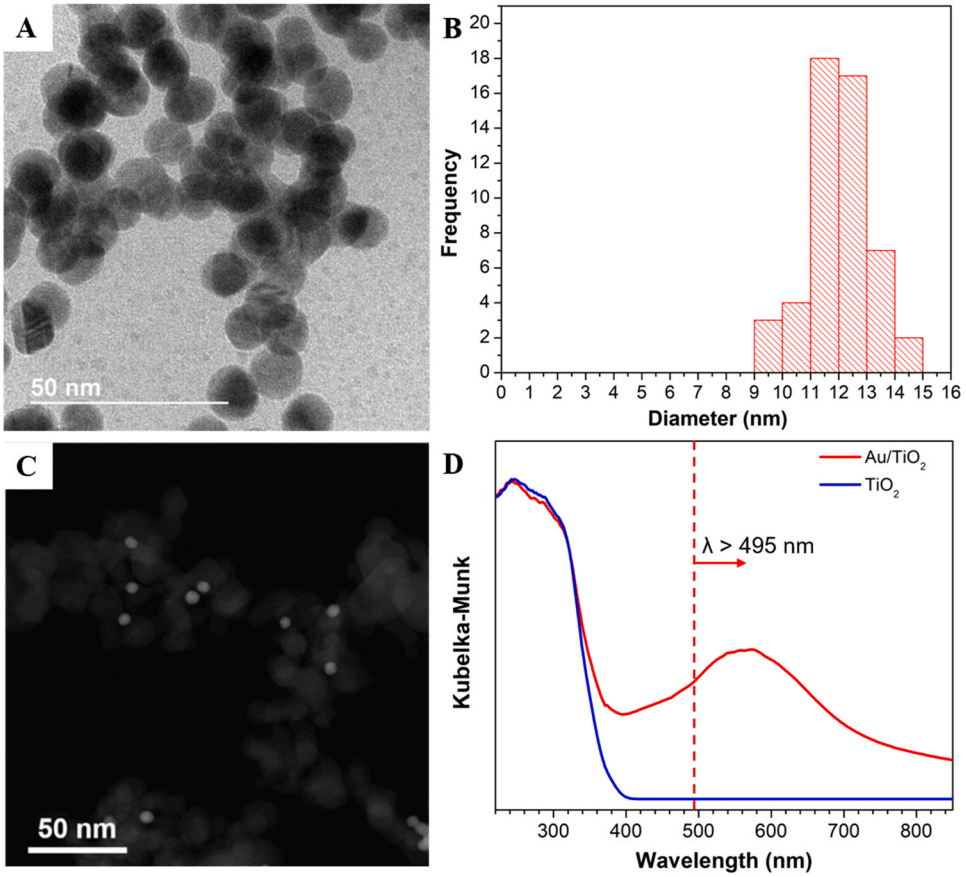

Fig. 1. Characterization of Au/TiO_2 plasmonic photocatalysts constructed via a colloidal photo-deposition method to load 5 wt% Au NPs onto TiO_2 supports (P25): (A) Representative transmission electron microscopy (TEM) image and (B) Diameter distribution of as-prepared Au NPs extracted from A. (C) High-angle annular dark-field scanning transmission electron microscopy (HAADF-STEM) image of Au/TiO_2 composite prepared by colloidal photo-deposition method, (D) UV-Vis diffuse reflectance spectra of Au/TiO_2 (red curve) and pure TiO_2 (blue curve) plotted against the optical edge of 495 nm long pass filters.

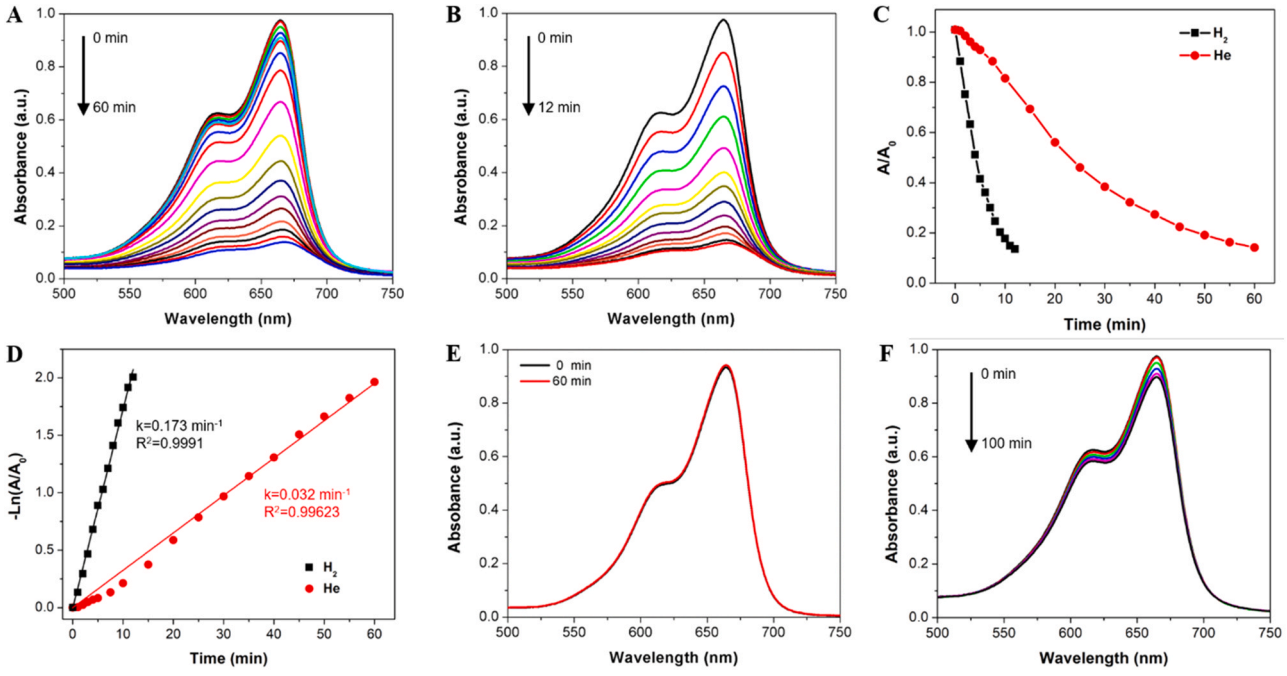

Fig. 2. Photocatalytic degradation of MB using Au/TiO_2 under visible light illumination ($\lambda > 495$ nm): Evolution of adsorption spectra of MB as a function of time over Au/TiO_2 (A) under He bubbling, (B) under H_2 bubbling, (C) Comparison of MB degradations (A/A_0) over time obtained by UV–vis absorbance at wavelength of 664 nm, (D) the photocatalytic degradation kinetics curve of MB, (E) MB absorbance in dark condition, (F) Photocatalytic degradation of MB in H_2 with addition of 1.0 mM TEOA (a quencher of h^+). a.u., arbitrary units.

distribution of prepared Au NPs is illustrated in Fig. 1B, exhibiting a mean value of 12 ± 3 nm. The HAADF-STEM in Fig. 1C also showed that the Au NPs were successfully dispersed and integrated on irregular TiO_2 (P25) substrate with well-defined size. Fig. 1D illustrates the UV–vis absorption spectra of the pure TiO_2 and Au/TiO_2. The pure TiO_2 showed strong and negligible absorption in the UV region and visible range (blue curve), respectively, with a sharp absorption edge near 400 nm due to inter-band electronic transition, which is consistent with the bandgap of anatase-rutile mixture of 3.0–3.2 eV. After depositing Au NPs, an additional absorption band centered at 568 nm corresponding to photon energy of 2.18 eV was observed at visible range around 400–700 nm in the spectrum (red curve), due to the SPR phenomenon. The color of catalyst powder also changes from white to dark purple. The characteristic SPR absorption band of Au NPs well matches the highest photon flux of solar spectrum and is distinguishable from excitation of TiO_2. The UV–vis absorption spectra also suggested that Au NPs have been successfully integrated to TiO_2 nanoparticles, and only SPR of Au NPs was excited in the heterostructure under visible light irradiation.

3.2. Photocatalytic activity

Photocatalytic degradation of MB was carried out over Au/TiO_2 upon visible irradiation to identify the contribution of H_2 on reactivity of photogenerated hot holes. A Xe lamp coupled with 495 nm cutoff-filter was utilized to rule out the contribution from TiO_2 (absorbance edge at ~400 nm) and oxygen was depleted by He or H_2 before the reaction to exclude possible electron-mediated superoxide (O_2^-) generation. Fig. 2A and B show that the most intense absorption peak of MB in visible region is at ~664 nm with a shoulder at ~612 nm, which are ascribed to MB monomer and dimer, respectively [27]. Upon visible illumination, the intensities of these absorption bands decrease gradually with increasing degradation time without revealing any new band, suggesting stable intermediate byproduct is unlikely to be generated. The photocatalytic activities of Au/TiO_2 in H_2 or He were further evaluated by the degradation of MB (A/A_0) as illustrated in Fig. 2C. The MB degradation reached approximately 91% after 12 min in H_2, and 90% after 60 min in He, respectively. To quantify the contribution of different adsorbates under visible light, simulated curves of the concentration of MB as a function of degradation time were presented in Fig. 2D. The kinetic curves for MB degradation are well fitted to the pseudo-first-order reaction kinetics equation according to Langmuir Hinshelwood model, namely, ($ln\ (C/C_0) = -kt$) [29]. The determined rate constant k is 0.173 min^{-1} for H_2, which is more than 5 times higher than that of He (0.032 min^{-1}), confirming an enhanced degradation of MB over Au/TiO_2 by introduction of H_2. In other words, presence of H_2 can significantly accelerate the MB degradation process over Au/TiO_2 composite under visible irradiation. Control experiments showed that negligible degradation of MB was achieved in the dark for 60 min with same catalysts (Fig. 2E) at the same temperature which excludes thermal catalytic degradation [33]. It should also be noted that *leuco* MB is less likely to form in large quantity in this neutral pH condition [30], evidenced by decrease of UV-Vis band intensity at 256 nm. Trapping experiments were conducted to identify the dominant species. As illustrated in Fig. 2F, the degradation process of MB obviously slowed down with addition of 1 mM TEOA (a quencher of h^+), confirming that plasmon-induced hot holes play a vital role in photocatalytic degradation of MB. By contrast, the degradation rate remains almost unchanged when 1.0 mM IPA (a quencher of·OH) was added. These results clearly indicate that incorporation of H_2 can dramatically enhance plasmonic hot hole-mediated photocatalysis. Previous studies [21,22] strongly suggested that the Au-H antibonding state formed between Au surface and atomic H can provide local electronic structure for hole trapping, which is expected to not only suppress recombination of charge carriers but also preserve oxidation power of hot holes. The evidence of the existence of atomic H as intermediate product will be further discussed in the following sessions.

3.3. Visible-light induced H_2 spillover

In situ diffuse reflectance infrared Fourier transform spectroscopy (DRIFTS) was exploited to demonstrate the existence of atomic H and pinpoint the physical location of active sites for hot hole trapping. Detection of the atomic H was accomplished by comparing the IR absorption of Au/TiO_2 in H_2 with and without visible light irradiation originated from H_2 spillover effect. It has been reported that a featureless broad IR absorption at 4000–1000 cm^{-1} can be observed when atomic H diffuses into TiO_2 lattice via an *n*-doping process [34]. Hence P25 TiO_2 substrate in Au/TiO_2 composite was used as a probe for detection of atomic H. Using cut-off filter of $\lambda > 495$ nm allows the selective excitation of the Au NPs while excluding any contribution from direct inter-band transitions within the TiO_2 support. Fig. 3 illustrated the IR spectrum for Au/TiO_2 sample in dark condition (blue line) after exposure to H_2 for 60 min at 30 °C, suggesting very weak H_2 spillover process driven by thermal dissociation. It has been reported that thermal H_2 dissociation occurs readily at room temperature on supported Au NPs with diameter of 2–3 nm [34]. In this study, the relative inertness was ascribed to the bigger size of ~12 nm of Au NPs. By contrast, pronounced features were observed after 60 min of visible light irradiation in H_2 (black curve in Fig. 3), clearly indicating that the process is directly driven by photo-excitation. Emerging of a band at around 3274 cm^{-1} and negative bands (~3658 cm^{-1} and ~3738 cm^{-1}) were observed. This indicates the diffusion of atomic H to react with surface oxygen on TiO_2 around the periphery of the Au NPs after H_2 dissociation on the Au NPs, generating surface Ti-OH groups whose IR signature could be broadened by hydrogen bond formation [34]. Moreover, a broad featureless IR absorption that ranges from 4000 to 1000 cm^{-1} was observed under visible-light irradiation in H_2, which rises from ~1000 cm^{-1} to a maximum at ~1750 cm^{-1} and then monotonically decreases toward the higher frequencies. This is ascribed to the formation of localized Ti-O(H)-Ti species which donate one electron to shallow trapped (ST) states slightly below the CB edge of TiO_2 [34]. These ST electrons can also be promoted into the continuum of the CB of TiO_2 by thermal energy. Both ST and CB electrons can generate broad featureless band in IR region by absorbing photons with corresponding energy. These evidences further confirmed the role of H_2: Upon exposure of the Au/TiO_2 to molecular H_2 under plasmonic excitation, H_2 molecules could dissociate into atomic H to adsorb on the surface of Au NPs and then diffuse to the TiO_2 substrate.

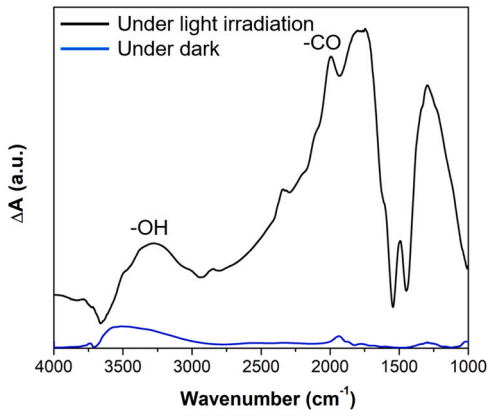

Fig. 3. *In situ* diffuse reflectance infrared Fourier transform spectroscopy (DRIFTS) spectra illustrating absorption changes (ΔA) during exposure of Au/TiO_2 composite to H_2 under $\lambda > 495$ nm visible light irradiation (black) and under dark condition (blue). Control experiment under dark condition showed that thermal-driven H_2 dissociation on Au/TiO_2 is very week.

3.4. Adsorbed CO as a molecule probe

Concomitant with light-induced H_2 spillover, we exploited the vibrational signatures of adsorbed carbon monoxide molecules, *v*CO(a), in the range of 2250–1900 cm^{-1}, to pinpoint the physical location of hot hole trapping upon visible-light irradiation by tracking the electronic character of the Au sites. Monitoring subtle changes in *v*CO(a) enabled the indirect observation of trapped hot holes at Au-H interfacial structures. Fig. 4A illustrated the DRIFTS spectra of pre-CO covered Au/TiO_2 at 30 °C. Two distinct vibrational modes were observed over Au/TiO_2 associated with surface-bound CO, and their peak positions were monitored as a function of time since exposure to H_2 (Fig. 4B). *v*CO(a) are known to be susceptible to subtle changes in the electronic character of Au surface, where Stark effect and π back-donation effect could contribute to *v*CO(a) shifts on charged Au NPs [34]. *v*CO(a) will shift to lower wavenumbers (red-shift) or higher wavenumbers (blue-shift) in accordance with an increase or decrease in electron density, respectively, on the Au NP [34]. The band that appears at 2108 cm^{-1} is ascribed to CO linearly adsorbed on neutral Au sites (Au^0) [32,35]. The peak position of this band basically remains unchanged throughout experiment. On the other hand, the band that initially appears at 2058 cm^{-1} and then shifts to 1996 cm^{-1}, is attributed to CO adsorbed at low coordinated positions (step/kink sites) on Au NPs, denoted by Au^{step}-CO [36]. These low coordinated positions were reported to locate away from the Au/TiO_2 interface [32]. It shows that *v*(Au^{step}-CO) is significantly affected by the presence of H_2 under visible illumination. As illustrated by the slope (blue curve) in Fig. 4B, the *v*(Au^{step}-CO) at 2058 cm^{-1} was red-shifted by 62 cm^{-1} in 65 min upon H_2 exposure, which obviously evidences the accumulation of negative electronic charge on Au^{step} surface species, supporting the assumption that positive hot holes were trapped at local Au-H interfacial structure while conferring a partial-negative charge to Au atoms nearby. In other words, trapped hot holes remain confined to the low coordination positions at surface of Au NPs under reaction conditions. Although one might argue that the red shift of *v*(Au^{step}-CO) could originate from the strong metal-support interaction between Au NPs and reduced TiO_2, where the electrons migrated from TiO_{2-x} to Au sites on the interfaces [35,37], this is against observation that *v*(Au^0-CO) remains largely unchanged (red curve in Fig. 4B). These results imply that low coordinated positions like steps and kinks at the surface of Au NPs are most likely the active sites for H_2 chemistry under visible light irradiation.

3.5. The d-band model analysis

To understand the electronic structure of Au-H interfacial binding at metallic surface of Au NPs, we first consider the interaction between H and Au outer layer orbitals under dark condition. The electronic interaction can be regarded as the coupling between the H1*s* valence state and the Au5*d* and 6 *s* states, resulting in splitting into bonding and antibonding states. The *s*-*s* interaction depends on adsorbate species, but it is rather consistent along the metals [38]. The interaction of the H1*s* state with the Au6*s* band is attractive because a filled deep-lying bonding state and an empty antibonding state are formed [22]. The *d*-part gives the metal-to-metal variability and comes from the *d*-band center and filling. The interaction of the renormalized state related to H (namely, H1*s*-Au6*s* bonding state) with the Au 5*d* band gives rise to a repulsion because the center of newly formed antibonding states are much lower than E_F and largely filled by electrons [22]. In addition, H_2 molecules cannot couple efficiently to the Au phonons due to the high mass of Au atoms and will therefore bounce off the surface without much loss of kinetic energy [2,25]. In other words, Au-H_2 interaction possesses both a filled H1*s*-Au5*d* antibonding state and the largest coupling matrix element. As a consequence, H_2 can only spend limited time on Au surface and interact weakly with Au surface under dark condition [25]. However, the hybridized H1*s*-Au5*d* antibonding states largely occupied by electrons are available to accept photogenerated hot holes from plasmonic Au NPs when irradiated by visible light at the presence of H_2. The continuous migration of plasmon-induced hot holes into the antibonding states can in return stabilize the Au-H interfacial structure due to an increased electron depletion of the antibonding state, leading to a stronger Au-H bond. Therefore, although Au-H interaction is weak due to filled antibonding state, it could be stabilized and available for hot hole trapping under light illumination. It is worth mentioning that holes formed in the *d*-band of Au by inter-band transitions are in principle potent enough to oxidize MB [3,4]. This study mainly focuses on intra-band hot holes generated by visible light (λ > 495 nm).

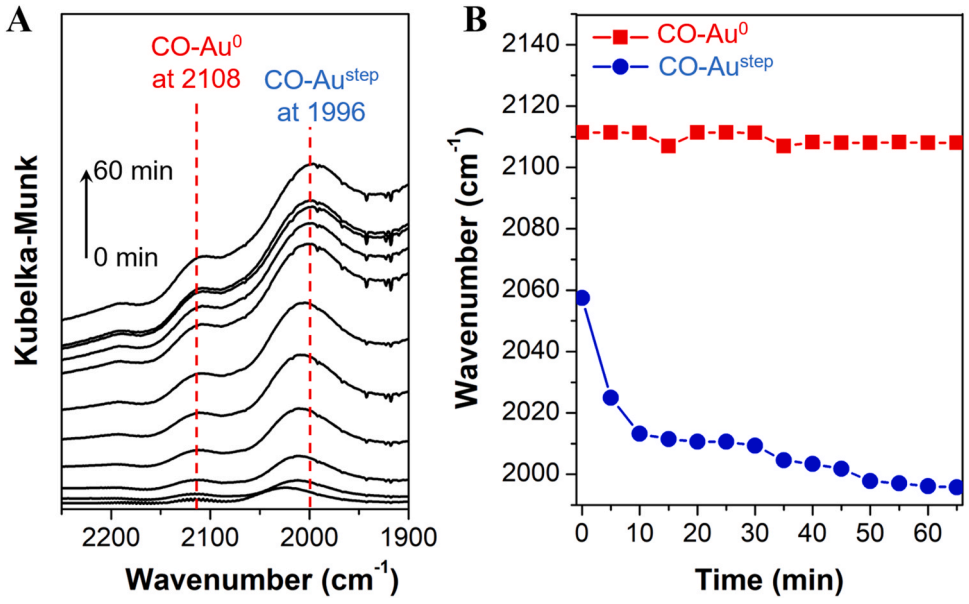

Fig. 4. CO-adsorption FTIR spectra of Au/TiO_2 composite under 1 atm molecular hydrogen (H_2) irradiated by λ > 495 nm visible light at 30 °C. (A) A series of DRIFTS spectra recorded to track the changes of CO vibration from 0 to 60 min; (B) The changes in the wavenumber of CO(a) stretching vibrations for CO molecules bonded to neutral Au sites (CO-Au^0) and low coordinated positions (CO-Au^{step}) in Au NPs with increasing exposure time in H_2.

3.6. Proposed photocatalytic mechanism

According to the above experimental results and theoretical analysis, a possible mechanism pathway for plasmonic hot hole migration and subsequent photocatalytic degradation of MB by Au/TiO_2 under visible irradiation is illustrated in Scheme 1. Upon plasmonic excitation, hot electron-hole pairs are generated from the interaction between free electrons on the Au surface and incoming radiation. In the absence of H_2, the hot holes suffer from ultrafast relaxation to energy levels close to E_F within 100 fs to 1 ps due to electron-electron scattering [2], leading to reduction of their oxidation power. By contrast, introduction of H_2 allows migration of plasmonic holes nearby to the Au-H hybridized antibonding states formed at low coordination positions on Au NPs, leading to the "trapping" of hot holes at Au-H interface that are available to convert MB into oxidation products. Such behavior is expected to not only prolong the lifetime of plasmon-induced hot holes, but also preserve their oxidation power due to following reasons:

(1) The hot electrons in Au NPs are reported to be largely delocalized with mean free path in the range of 20–150 nm [39,40], whereas plasmon-induced hot holes are trapped at Au-H interfacial structures located at the low coordinated positions of Au NPs (e.g., step, kink and other defect sites). This discrepancy can significantly improve spatial separation of photogenerated hot electrons and holes to suppress charge recombination.
(2) The relaxation of plasmon-induced hot holes to energy level close to E_F is extremely fast [2,10,12]. As a consequence, those hot holes are not thermodynamically favorable for uphill reactions. Since the center of the hybridized *s-d* antibonding states of Au-H is much lower (e.g. ~0.6 eV in previous studies) than E_F of Au NPs, [22] the trapped hot holes are very likely to possess higher oxidation power than the naturally relaxed hot holes.

These benefits to improve hot hole utilization efficiency offers considerable advantages for plasmonic photocatalysis, due to the asymmetrical energy distribution between hot electrons and holes relative to E_F [12,41], which indicate photogenerated hot holes have more energetic kinetics compared to hot electrons. It's also worth mentioning that the size of atomic H is so small that it is unlikely to block MB from accessing Au surface, which confirms the feasibility of above design. A number of photocatalytic reactions facilitated by hot holes could be accelerated by this strategy. Specific examples include metal oxidation [16], nano-deposition [17], oxygen generation [18], and methane oxidation [42].

4. Conclusion

A novel metal-adsorbate interfacial structure was designed in present study to convert the unusable hot holes into "effective" ones that could be efficiently exploited in photocatalytic reactions. Superior photocatalytic activity of MB degradation over Au/TiO_2 was observed in the presence of H_2 under visible light irradiation. >90% of MB photodegradation was achieved in H_2 in 12 min (0.173 min^{-1}) which is >5 times faster than that in He (0.032 min^{-1}). Visible-light-induced H_2 spillover characterized by *in situ* FTIR demonstrated the existence of atomic H under plasmonic excitation, which provides strong evidence of formation of Au-H interfacial structure acting as trapping sites of plasmonic holes. DRIFTS coupled with CO molecular probe reveals that hot hole trapping is preferably located on the low coordinated positions of Au NPs. The *d*-band model analysis predicts the antibonding states of H1*s* - Au5*d* hybridization on Au surface to effectively suppress electron-hole recombination and preserve oxidation power of plasmonic hot holes. This proof-of-concept design not only enables spectroscopically viewing spatial location of trapped hot holes in Au NPs under plasmon excitation, but also increases generation of "effective" hot holes capable of participating in plasmonic photochemistry under reaction conditions.

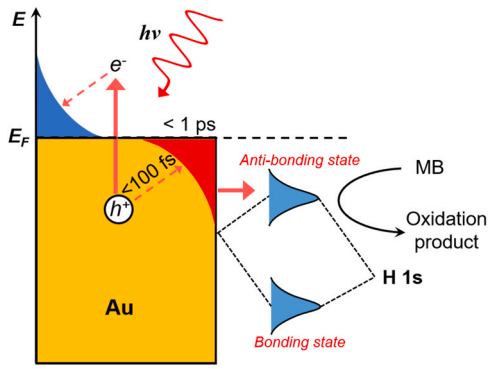

Scheme 1. A schematic diagram of proposed key processes for plasmonic hole mediated photodegradation over Au NPs under visible light. Visible-light-generated hot holes transfer from a photoexcited Au NP to the hybridized *s-d* antibonding state of Au-H interfacial structure, which not only prolong the lifetime of plasmon-induced hot holes, but also preserve their oxidation power, leading to enhanced photocatalytic activity.

CRediT authorship contribution statement

Chaoyu Li: Conceptualization, Writing – original draft, Methodology, Software, Data curation. **Zhiling Ma:** Writing – review & editing. **Bing Han**: Supervision, Validation, Writing – review & editing.

Declaration of Competing Interest

The authors declare that they have no known competing financial interests or personal relationships that could have appeared to influence the work reported in this paper.

Acknowledgements

This work was financially supported by Victoria-Jiangsu Program for Technology and Innovation Research and Development (VIC-JS TECH) project "Development of novel bio-organic fertilisers", Research Innovation Team of College of Chemistry and Environmental Science of Hebei University (hxkytd-py2104), National Natural Science Foundation of China (22002032), Hebei Key R&D Program (20327303D), Natural Science Foundation of Hebei Province (B2019201064), and The Excellent Going Abroad Experts' Training Program in Hebei Province (202001).

Appendix A. Supporting information

Supplementary data associated with this article can be found in the online version at doi:10.1016/j.apcatb.2021.120901.

References

[1] C. Zhang, F. Jia, Z. Li, X. Huang, G. Lu, Plasmon-generated hot holes for chemical reactions, Nano Res. 13 (12) (2020) 3183–3197.
[2] M.L. Brongersma, N.J. Halas, P. Nordlander, Plasmon-induced hot carrier science and technology, Nat. Nanotechnol. 10 (1) (2015) 25–34.
[3] Y. Kim, J.G. Smith, P.K. Jain, Harvesting multiple electron–hole pairs generated through plasmonic excitation of Au nanoparticles, Nat. Chem. 10 (7) (2018) 763–769.
[4] S. Yu, P.K. Jain, Plasmonic photosynthesis of C1–C3 hydrocarbons from carbon dioxide assisted by an ionic liquid, Nat. Commun. 10 (1) (2019) 2022.
[5] S.M. Barnett, K.I. Goldberg, J.M. Mayer, A soluble copper–bipyridine water-oxidation electrocatalyst, Nat. Chem. 4 (6) (2012) 498–502.
[6] Z. Lian, M. Sakamoto, H. Matsunaga, J.J.M. Vequizo, A. Yamakata, M. Haruta, H. Kurata, W. Ota, T. Sato, T. Teranishi, Near infrared light induced plasmonic hot hole transfer at a nano-heterointerface, Nat. Commun. 9 (1) (2018) 1–7.
[7] D. Mateo, I. Esteve-Adell, J. Albero, J.F.S. Royo, A. Primo, H. Garcia, 111 oriented gold nanoplatelets on multilayer graphene as visible light photocatalyst for overall water splitting, Nat. Commun. 7 (2016) 11819.

[8] S.-F. Hung, F.-X. Xiao, Y.-Y. Hsu, N.-T. Suen, H.-B. Yang, H.M. Chen, B. Liu, Iridium oxide-assisted plasmon-induced hot carriers: improvement on kinetics and thermodynamics of hot carriers, Adv. Energy Mater. 6 (8) (2016) 1501339.
[9] J. Sa, G. Tagliabue, P. Friedli, J. Szlachetko, M.H. Rittmann-Frank, F. G. Santomauro, C.J. Milne, H. Sigg, Direct observation of charge separation on Au localized surface plasmons, Energy Environ. Sci. 6 (12) (2013) 3584–3588.
[10] A.M. Brown, R. Sundararaman, P. Narang, W.A. Goddard, H.A. Atwater, Nonradiative plasmon decay and hot carrier dynamics: effects of phonons, surfaces, and geometry, ACS Nano 10 (1) (2016) 957–966.
[11] J.R. Dunklin, A.H. Rose, H. Zhang, E.M. Miller, J. van de Lagemaat, Plasmonic hot hole transfer in gold nanoparticle-decorated transition metal dichalcogenide nanosheets, ACS Photonics 7 (1) (2020) 197–202.
[12] R. Sundararaman, P. Narang, A.S. Jermyn, W.A., I.I.I. Goddard, H.A. Atwater, Theoretical predictions for hot-carrier generation from surface plasmon decay, Nat. Commun. 5 (2014) 5.
[13] E.S. Thrall, A. Preska Steinberg, X. Wu, L.E. Brus, The role of photon energy and semiconductor substrate in the plasmon-mediated photooxidation of citrate by silver nanoparticles, J. Phys. Chem. C 117 (49) (2013) 26238–26247.
[14] T. Peng, J. Miao, Z. Gao, L. Zhang, Y. Gao, C. Fan, D. Li, Reactivating catalytic surface: Insights into the role of hot holes in plasmonic catalysis, Small 14 (2018) 12.
[15] L. He, C. Liu, J. Tang, Y. Zhou, H. Yang, R. Liu, J. Hu, Self-catalytic stabilized Ag-Cu nanoparticles with tailored sers response for plasmonic photocatalysis, Appl. Surf. Sci. 434 (2018) 265–272.
[16] G. Lu, H. Yuan, L. Su, B. Kenens, Y. Fujita, M. Chamtouri, M. Pszona, E. Fron, J. Waluk, J. Hofkens, H. Uji-i, Plasmon-mediated surface engineering of silver nanowires for surface-enhanced Raman scattering, J. Phys. Chem. Lett. 8 (13) (2017) 2774–2779.
[17] S. Wang, Y. Gao, S. Miao, T. Liu, L. Mu, R. Li, F. Fan, C. Li, Positioning the water oxidation reaction sites in plasmonic photocatalysts, J. Am. Chem. Soc. 139 (34) (2017) 11771–11778.
[18] L. Wang, H. Hu, N.T. Nguyen, Y. Zhang, P. Schmuki, Y. Bi, Plasmon-induced hole-depletion layer on hematite nanoflake photoanodes for highly efficient solar water splitting, Nano Energy 35 (2017) 171–178.
[19] T. Tatsuma, H. Nishi, Plasmonic hole ejection involved in plasmon-induced charge separation, Nanoscale Horiz. 5 (2020) 597–606.
[20] A.J. Cowan, J.R. Durrant, Long-lived charge separated states in nanostructured semiconductor photoelectrodes for the production of solar fuels, Chem. Soc. Rev. 42 (6) (2013) 2281–2293.
[21] K. Nørskov Jens, F. Abild-Pedersen, F. Stud, T. Bligaard, T. Campbell Charles, Density functional theory in surface chemistry and catalysis, Proc. Natl. Acad. Sci. USA 108 (3) (2011) 937–943.
[22] B. Hammer, J.K. Norskov, Why gold is the noblest of all the metals, Nature 376 (6537) (1995) 238–240.
[23] H. Zhang, X.-G. Zhang, J. Wei, C. Wang, S. Chen, H.-L. Sun, Y.-H. Wang, B.-H. Chen, Z.-L. Yang, D.-Y. Wu, J.-F. Li, Z.-Q. Tian, Revealing the role of interfacial properties on catalytic behaviors by in situ surface-enhanced Raman spectroscopy, J. Am. Chem. Soc. 139 (2017) 10339–10346.
[24] X.-F. Yang, A. Wang, B. Qiao, J. Li, J. Liu, T. Zhang, Single-atom catalysts: a new frontier in heterogeneous catalysis, Acc. Chem. Res. 46 (8) (2013) 1740–1748.
[25] S. Mukherjee, L. Zhou, A.M. Goodman, N. Large, C. Ayala-Orozco, Y. Zhang, P. Nordlander, N.J. Halas, Hot-electron-induced dissociation of H_2 on gold nanoparticles supported on SiO_2, J. Am. Chem. Soc. 136 (1) (2014) 64–67.
[26] D. Sil, K.D. Gilroy, A. Niaux, A. Boulesbaa, S. Neretina, E. Borguet, Seeing is believing: Hot electron based gold nanoplasmonic optical hydrogen sensor, ACS Nano 8 (8) (2014) 7755–7762.
[27] S. Mondal, M.E. De Anda Reyes, U. Pal, Plasmon induced enhanced photocatalytic activity of gold loaded hydroxyapatite nanoparticles for methylene blue degradation under visible light, RSC Adv. 7 (14) (2017) 8633–8645.
[28] A. Tanaka, A. Ogino, M. Iwaki, K. Hashimoto, A. Ohnuma, F. Amano, B. Ohtani, H. Kominami, Gold-titanium(IV) oxide plasmonic photocatalysts prepared by a colloid-photodeposition method: Correlation between physical properties and photocatalytic activities, Langmuir 28 (36) (2012) 13105–13111.
[29] Z. Ma, Q. Jia, C. Tao, B. Han, Highlighting unique function of immobilized superoxide on TiO_2 for selective photocatalytic degradation, Sep. Purif. Technol. 13 (2020) 238.
[30] C. Tao, Q. Jia, B. Han, Z. Ma, Tunable selectivity of radical generation over TiO_2 for photocatalysis, Chem. Eng. Sci. 214 (2020) 214.
[31] Z. Ma, Q. Jia, Y. Shi, X. Duan, B. Han, Synergistic effect of aeration-assisted photocatalysis: Two parallel mechanism pathways for TXP-10 surfactant removal, J. Water Process. Eng. 38 (2020) 38.
[32] J. Zhang, H. Wang, L. Wang, S. Ali, C. Wang, L. Wang, X. Meng, B. Li, D.S. Su, F.-S. Xiao, Wet-chemistry strong metal-support interactions in titania-supported Au catalysts, J. Am. Chem. Soc. 141 (7) (2019) 2975–2983.
[33] Y. Dubi, I.W. Un, Y. Sivan, Thermal effects – an alternative mechanism for plasmon-assisted photocatalysis, Chem. Sci. 11 (19) (2020) 5017–5027.
[34] D.A. Panayotov, S.P. Burrows, J.T. Yates, J.R. Morris, Mechanistic studies of hydrogen dissociation and spillover on Au/TiO_2: IR spectroscopy of coadsorbed CO and H-donated electrons, J. Phys. Chem. C 115 (45) (2011) 22400–22408.
[35] H. Tang, Y. Su, B. Zhang, A.F. Lee, M.A. Isaacs, K. Wilson, L. Li, Y. Ren, J. Huang, M. Haruta, B. Qiao, X. Liu, C. Jin, D. Su, J. Wang, T. Zhang, Classical strong metal–support interactions between gold nanoparticles and titanium dioxide, Sci. Adv. 3 (10) (2017), e1700231.
[36] J. Luo, Y. Liu, Y. Niu, Q. Jiang, R. Huang, B. Zhang, D. Su, Insight into the chemical adsorption properties of CO molecules supported on Au or Cu and hybridized Au-CuO nanoparticles, Nanoscale 9 (39) (2017) 15033–15043.
[37] Y. Wang, D. Widmann, M. Heenemann, T. Diemant, J. Biskupek, R. Schlögl, R. J. Behm, The role of electronic metal-support interactions and its temperature dependence: CO adsorption and CO oxidation on Au/TiO_2 catalysts in the presence of TiO_2 bulk defects, J. Catal. 354 (2017) 46–60.
[38] R. García-Muelas, N. López, Statistical learning goes beyond the *d*-band model providing the thermochemistry of adsorbates on transition metals, Nat. Commun. 10 (1) (2019) 4687.
[39] M.P. Seah, W.A. Dench, Quantitative electron spectroscopy of surfaces: a standard data base for electron inelastic mean free paths in solids, Surf. Interface Anal. 1 (1) (1979) 2–11.
[40] K.W. Frese, C. Chen, Theoretical models of hot carrier effects at metal-semiconductor electrodes, J. Electrochem. Soc. 139 (11) (1992) 3234–3243.
[41] H. Lee, K. Song, M. Lee, J.Y. Park, In situ visualization of localized surface plasmon resonance-driven hot hole flux, Adv. Sci. 7 (20) (2020) 2001148.
[42] Z. Ma, W. Liu, W. Yang, W. Li, B. Han, Temperature effects on redox potentials and implications to semiconductor photocatalysis, Fuel 286 (2021), 119490.
[43] X. Hao, Q. Guo, M. Li, Z. Jin, Y. Wang, TiO_2 as an interfacial-charge-transfer-bridge to construct eosin Y-mediated direct Z-scheme electron transfer over a Co_9S_8 quantum dot/TiO_2 photocatalyst, Catal. Sci. Technol. 10 (2020) 5267–5280.